Thermally Activated Upconversion Near-Infrared Photoluminescence from Carbon Dots Synthesized via Microwave Assisted Exfoliation

Di Li, Chao Liang, Elena V. Ushakova, Minghong Sun, Xiaodan Huang, Xiaoyu Zhang, Pengtao Jing, Seung Jo Yoo, Jin-Gyu Kim, Enshan Liu, Wei Zhang, Lihong Jing, Guichuan Xing, Weitao Zheng, Zikang Tang, Songnan Qu,* and Andrey L. Rogach

Upconversion near-infrared (NIR) fluorescent carbon dots (CDs) are important for imaging applications. Herein, thermally activated upconversion photoluminescence (UCPL) in the NIR region, with an emission peak at 784 nm, which appears under 808 nm continuous-wave laser excitation, are realized in the NIR absorbing/emissive CDs (NIR-CDs). The NIR-CDs are synthesized by microwave-assisted exfoliation of red emissive CDs in dimethylformamide, and feature single or few-layered graphene-like cores. This structure provides an enhanced contact area of the graphene-like plates in the core with the electron-acceptor carbonyl groups in dimethylformamide, which contributes to the main NIR absorption band peaked at 724 nm and a tail band in 800–850 nm. Temperature-dependent photoluminescence spectra and transient absorption spectra confirm that the UCPL of NIR-CDs is due to the thermally activated electron transitions in the excited state, rather than the multiphoton absorption process. Temperature dependent upconversion NIR luminescence imaging is demonstrated for NIR-CDs embedded in a polyvinyl pyrrolidone film, and the NIR upconversion luminescence imaging in vivo using NIR-CDs in a mouse model is accomplished.

Luminescence imaging in the near-infrared (NIR) spectral range from 700 to 1700 nm is of significance for in vivo studies, owing to the advantages of the deep tissue penetration

and reduced autofluorescence; this calls for development of luminophores featuring both the absorption and emission in the NIR region.[1] Comparing with the Stokes-shifted photoluminescence (SPL) commonly observed for the most of luminescent materials, upconversion photoluminescence (UCPL) represents short-wavelength emission, which occurs under long-wavelength excitation; it avoids the background from the Stokes fluorescence interference and thus offers a higher signal-to-background ratio in luminescence imaging.[2] Moreover, UCPL in the NIR spectral region is preferred for in vivo luminescence imaging as compared with upconversion to the visible region because of the greater penetration depth of both excitation and emission light into and from the biological tissue. UCPL can take place in a number of systems, such as lanthanide (Ln^{3+})-doped nanoparticles,[3] organic dyes,[4] and inorganic quantum dots[5] by utilization of additional photons or heat. Ln^{3+}-doped nanoparticles represent an established class of UCPL materials operating on the basis of the unique electronic

Dr. D. Li, M. Sun, Dr. P. Jing
State Key Laboratory of Luminescence and Applications
Changchun Institute of Optics
Fine Mechanics and Physics
Chinese Academy of Sciences
3888 Eastern South Lake Road, Changchun 130033, P. R. China
C. Liang, E. Liu, Prof. G. Xing, Prof. Z. Tang, Prof. S. Qu
Joint Key Laboratory of the Ministry of Education
Institute of Applied Physics and Materials Engineering
University of Macau
Avenida da Universidade
Taipa, Macau 999078, P. R. China
E-mail: songnanqu@um.edu.mo
Dr. E. V. Ushakova, Prof. A. L. Rogach
Center of Information Optical Technologies
ITMO University
Saint Petersburg 197101, Russia

The ORCID identification number(s) for the author(s) of this article can be found under https://doi.org/10.1002/smll.201905050.

DOI: 10.1002/smll.201905050

X. Huang, Dr. L. Jing
Key Laboratory of Colloid
Interface and Chemical Thermodynamics
Institute of Chemistry
Chinese Academy of Sciences
Bei Yi Jie 2, Zhong Guan Cun, Beijing 100190, P. R. China
Dr. X. Zhang, W. Zhang, Prof. W. Zheng
School of Materials Science and Engineering
Electron Microscopy Center
Jilin University
Changchun 130012, P. R. China
S. J. Yoo, Dr. J.-G. Kim
Department of Electron Microscopy Research
Korea Basic Science Institute
Daejeon 34133, South Korea
Prof. A. L. Rogach
Department of Materials Science and Engineering
and Centre for Functional Photonics (CFP)
City University of Hong Kong
Kowloon, Hong Kong S.A.R.

structure of Ln^{3+}, but they suffer from limitations of concentration quenching.[6] The UCPL of organic dyes and inorganic quantum dots is mostly realized through simultaneous absorption of multiple photons, which requires femtosecond (fs) laser excitation generated by an expensive equipment. In a few cases, thermally facilitated lower energy photon absorption can contribute to the UCPL in these systems,[4b,7] but such type of materials with near-infrared upconversion photoluminescence (NIR UCPL) is quite rare.

Carbon dots (CDs) represent a new kind of promising nanomaterials suitable for a variety of bioapplications, due to their well-documented biocompatibility and ease of surface functionalization.[8] Very recently, photoluminescence (PL) of CDs has been extended toward the NIR spectral region,[9] and several CD systems were reported to possess the capability of multiphoton induced UCPL under the excitation of fs pulse laser.[9a,d,10] Sun and co-workers reported CDs exhibiting bright two-photon visible luminescence under 800 nm excitation, and demonstrated the two-photon luminescence microscopy imaging of the CDs internalized in cancer cells.[10a] Lin and co-workers observed an excitation-independent two-photon fluorescence of CDs with λ_{max} = 683 nm under excitation from the fs pulse laser varying from 800 to 1000 nm.[10b] Yang and co-workers reported red and NIR emissive CDs with two-photon fluorescence (at 660 nm with a shoulder peak at 701 nm) under excitation of 800 nm fs pulse laser.[9d] We have recently demonstrated simultaneous two-photon-induced NIR emission and three-photon-induced red emission of CDs in dimethyl sulfoxide (DMSO) excited by a 1400 nm fs-laser.[9a] So far, examples of CDs featuring NIR UCPL have been rather rare, and their UCPL originated from multiphoton absorption process requiring the use of fs pulse laser excitation generated by an expensive equipment. Thus, developing CDs showing NIR UCPL under easy-to-realize, conventional NIR lighting source would be quite a breakthrough in this field.

In this work, we demonstrate thermally activated UCPL in the NIR region with a peak at 784 nm under 808 nm continuous-wave (CW) laser excitation using a new kind of NIR absorbing/emissive CDs (NIR-CDs). The NIR-CDs were synthesized from the red emissive CDs through a microwave-assisted exfoliation in dimethylformamide (DMF), forming single or few-layered graphene-like cores. These exfoliated graphene-like cores offer an enhanced contact area with DMF molecules which contain an electron-acceptor carbonyl group, leading to main NIR absorption band peaked at 724 nm and a tail band in 800–850 nm. Temperature dependent PL and transient absorption (TA) measurements show how thermally activated electron transitions in the excited state of NIR-CDs contribute to the UCPL. A temperature-dependent NIR upconversion luminescence imaging has been demonstrated with the NIR-CDs embedded in a polyvinyl pyrrolidone (PVP) films, and the NIR upconversion luminescence imaging in vivo using these NIR-CDs has been performed.

NIR-CDs were synthesized via a microwave-assisted heating of DMF solution (100 mL) of the red emissive CDs (R-CDs, 5 mg) at 100 °C for 70 min under atmospheric pressure. R-CDs have been conveniently synthesized via a solvothermal route following our previously reported procedure (see Supporting Information for detail).[9a] The resulting solution of NIR-CDs was concentrated in a rotary evaporator and washed with ethanol twice to obtain black powder of NIR-CDs. Transmission electron microscopy (TEM) and atomic force microscopy (AFM) were used to characterize the morphology and size distribution of the resulting NIR-CDs. TEM image (**Figure 1**a) shows circular shaped NIR-CDs with diameters in the range of 2–6 nm (average size: ~4 nm, Figure 1b). High-resolution TEM (HRTEM) image (Figure 1c) shows crystalline lattice fringes with a spacing of 0.21 nm, corresponding to the *d*-spacing of graphene {1$\bar{1}$00} planes.[9a,11] The topographic heights of
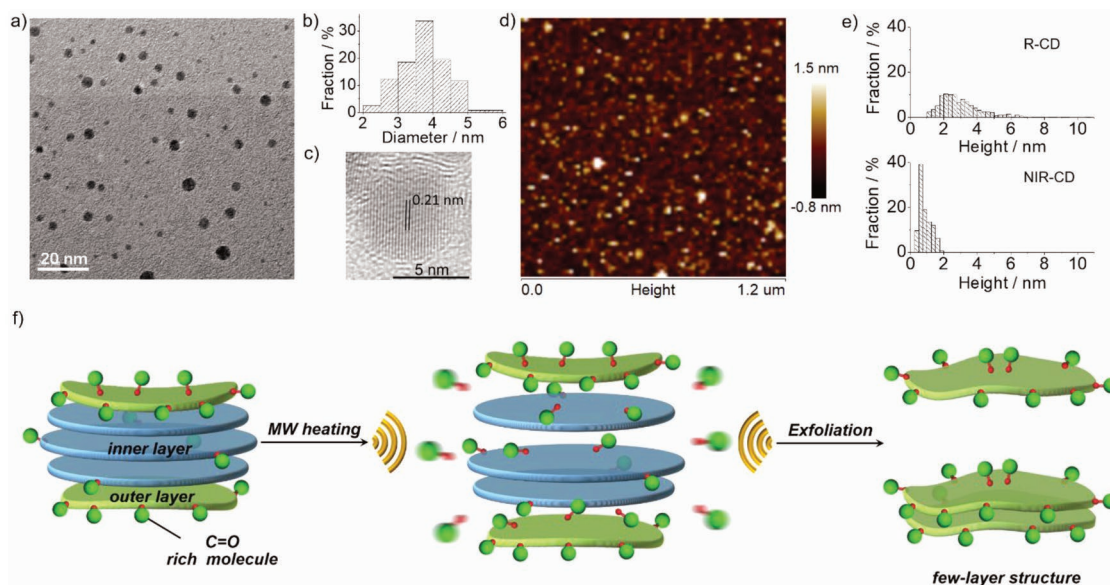
Figure 1. a) TEM image, b) size distribution, and c) HRTEM image of NIR-CDs. d) AFM image of NIR-CDs, with e) height distribution profiles of R-CDs (upper frame) and NIR-CDs (bottom frame). f) Schematics of the formation process of NIR-CDs through the microwave (MW)-assisted exfoliation of R-CDs.
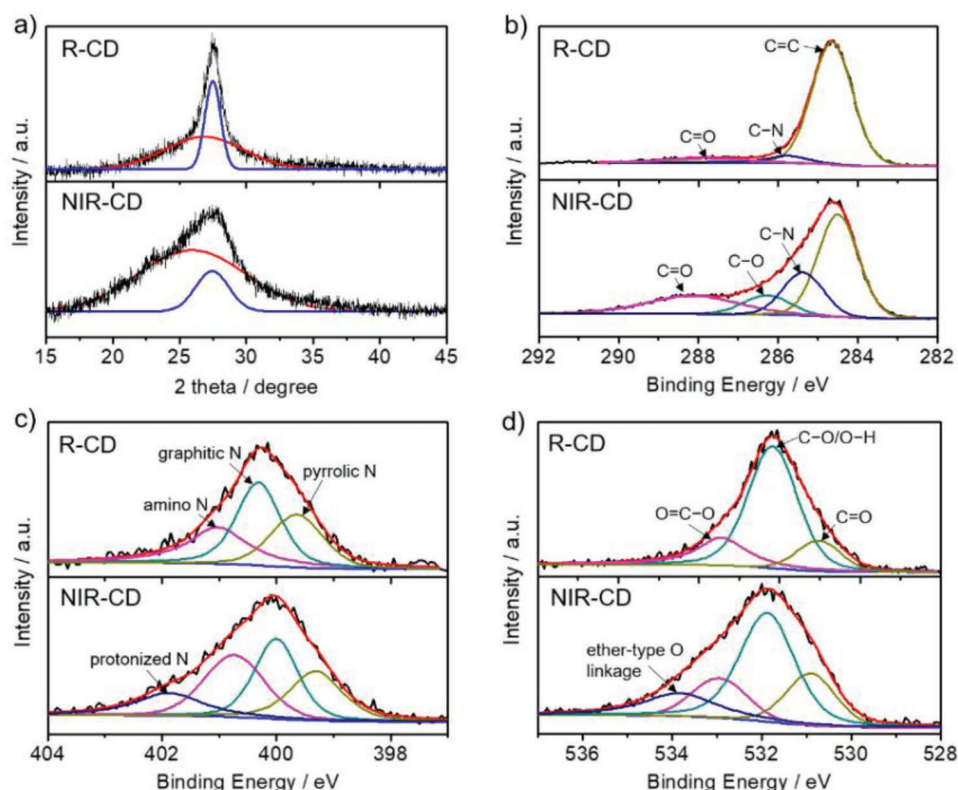
Figure 2. a) XRD profiles and b–d) high-resolution XPS spectra for (b) C 1s, (c) N 1s, and (d) O 1s elements of R-CDs (upper frames) and NIR-CDs (bottom frames).

NIR-CDs obtained from the AFM images (Figure 1d,e) are within the range of 0.4–2.0 nm (average height: 0.9 nm), corresponding to 1–3 graphene-like layer stacking in the cores.[12] These heights of NIR-CDs are significantly lower than those of R-CDs (average height: 3.0 nm as shown in Figure 1e), indicating that NIR-CDs are exfoliated from R-CDs forming one or few layers of graphene-like cores.

X-ray powder diffraction (XRD) and X-ray photoelectron spectroscopy (XPS) of NIR-CDs were performed to further study the structural/composition evolution from R-CDs to NIR-CDs. Different from the XRD pattern of R-CDs, which has a dominant sharp peak at 27.5° and a broad weaker band at 26.8°, the XRD pattern of the NIR-CDs exhibits a much weaker and broader peak at 27.5°, while a broader component centered at a smaller angle of 26.0° becomes dominant (**Figure 2**a). It can be inferred that the exfoliated single or few layer structure of NIR-CDs has a rather disordered layer stacking as compared to more compact structure of R-CDs. Deconvoluted high-resolution C 1s, N 1s, O 1s XPS spectra (Figure 2b–d) confirm the existence of C=C (284.5 eV), C−N (285.4 eV), C−O (286.3 eV), and O=C−O (288.1 eV) for C 1s; pyrrolic N (399.5 eV), graphitic N (400.2 eV), amino N (401 eV), and protonated N (402 eV) for N 1s; C=O (530.9 eV), C−O/O−H (531.9 eV), O=C−O (533.1 eV), and ether-type oxygen bonds (533.9 eV) for O 1s in the NIR-CDs.[13] We note that some of these components, such as C−O (286.3 eV), O=C−O (288.1 eV), protonated N (402 eV), and ether-type oxygen bonds (533.9 eV), occur at higher binding energy in the XPS spectra of NIR-CDs in comparison

with those of R-CDs (Figure 2b–d), indicating the increased amount of C, N, and O elements in higher oxidation state in NIR-CDs after microwave treatment of R-CDs. Based on the data listed above, a plausible formation mechanism of NIR-CDs is provided in Figure 1f. DMF is chosen as a solvent for the exfoliation of R-CDs because its electron-accepting carbonyl group can attach on the CD skeleton and disrupt the ordered layer-stacking structure of the R-CDs.[9a] Intermolecular interactions of the DMF molecules with R-CDs combined with the microwave heating treatment enable to exfoliate multilayered R-CDs. Upon microwave heating, the R-CDs with graphite-like cores are exfoliated into NIR-CDs with one-to-three layered graphene-like cores which are partially in a higher oxidation state due to the interactions with electron-acceptor carbonyls in DMF molecules.

The major absorption peak of R-CDs in DMF occurs at 619 nm, with an additional NIR absorption band at 720 nm. By contrast, the absorption spectrum of NIR-CDs in DMF exhibits a prominent NIR maximum at 724 nm, two weaker absorption bands at around 570 and 670 nm, and a tail band at 800–850 nm (**Figure 3**a). Furthermore, NIR-CDs in DMF exhibit an NIR emission peak at 770 nm under 732 nm excitation (Figure 3a), with a PL quantum yield (QY) of 11%. At the current state-of-the-art, the PL QY of 11% is a rather high value for NIR-emissive CDs which can be efficiently excited by NIR light.[9c,d] In our previous work, it has been demonstrated that molecules or polymers rich in sulfoxide/carbonyl groups can attach to the outer layers and the edges of the R-CDs, which
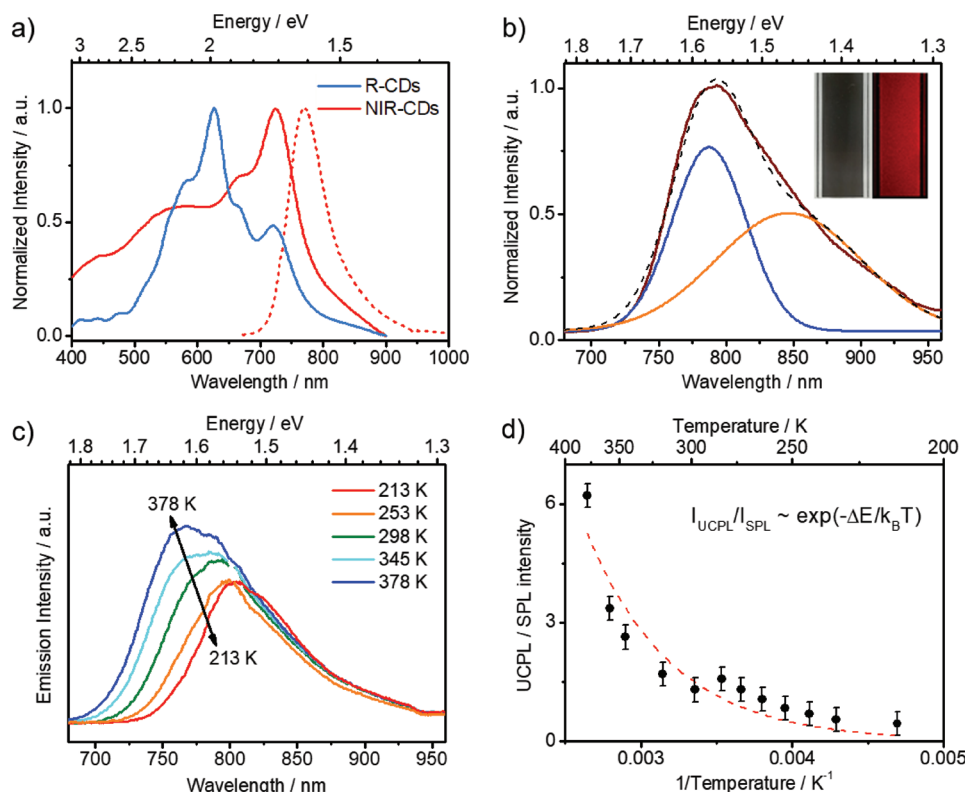
Figure 3. a) Absorption spectra (solid lines) of R-CDs and NIR-CDs, and PL spectra of NIR-CDs (dashed line) in DMF. b) UCPL spectrum of NIR-CDs in DMF under 808 nm laser excitation; the excitation peak at 808 has been artificially removed by subtracting the Gaussian peak with FWHM of 2.5 nm from the measured spectrum, which is shown in Figure S1 of the Supporting Information. The spectrum was decomposed by two Gaussians: UCPL band centered at 785 nm (blue line) and SPL band centered at 845 nm (orange line). The inset shows the bright field image (left) and the upconversion luminescence image (right) of NIR-CDs in DMF, acquired through a 770 nm shortpass optical filter under 808 nm excitation. c) Typical temperature dependent emission spectra of NIR-CDs in DMF taken under 808 nm laser excitation during the heating and cooling processes in the range of temperatures indicated on the frame. d) Temperature dependence of the integrated emission intensity ratio of UCPL and SPL bands.

results in increased surface oxidation and contributes to the NIR absorption band and fluorescence (λ_{abs}: ≈715–724 nm, λ_{em}: ≈750–760 nm) of R-CDs in solvents such as DMSO and DMF.[9a] Herein, microwave heating exfoliates multilayered π-conjugated cores of R-CDs into single-to-few-layer cores of NIR-CDs, which means nearly all the graphene-like plates in NIR-CDs can directly contact with solvent molecules. The absorption band in the red spectral region of NIR-CDs, corresponding to the absorption of the inner layers of cores, is relatively weak, demonstrating the exfoliated cores with no or few inner layers. Thus far, interaction of DMF molecules with outer layers of NIR-CDs becomes dominate and contributes to their main absorption band located at 724 nm. Besides the NIR PL under 732 nm excitation, UCPL occurs at 784 nm under the excitation of 808 nm CW laser in the DMF solution of NIR-CDs (Figure 3b; Figure S1, Supporting Information). The PL spectrum can be described as a sum of two bands: UCPL band at ≈760–800 nm and SPL band at ≈820–880 nm. To the best of our knowledge, the NIR UCPL has been for the first time observed in CD systems under CW laser excitation. The dependence of PL intensity at 780 nm on the excitation intensity at 808 nm shows a slope equal to one in linear fitting (plotted on a double logarithmic scale, see Figure S2, Supporting Information), suggesting that only one photon absorption is involved in the

upconversion process, rather than the common multiphoton absorption process.

In order to further explore the mechanism of the UCPL, temperature dependent UCPL spectra of NIR-CDs in DMF have been collected, and presented in Figure 3c and Figure S3 (Supporting Information). Upon heating the DMF solution of NIR-CDs from room temperature up to 378 K, the UCPL intensity increased and peak position blue-shifted gradually reaching 765 nm at 378 K. Conversely, upon cooling the solution from room temperature down to 213 K, the UCPL band gradually disappeared along with the gradually enhanced SPL band, which became dominant at 825 nm at 213 K. During the heating process, the absorption band of NIR-CDs in DMF slightly weakened, which was accompanied by a slight broadening and blue-shift (Figure S4a, Supporting Information). Neither increase of absorption nor obvious broadening of the absorption spectra was observed in the long wavelength region (680–900 nm), indicating that heating did not induce the Boltzmann distributions among higher vibrational levels (hot band) of the ground state. We note that under 732 nm excitation both SPL bands at ≈760–800 and ≈820–880 nm became enhanced when the temperature decreased from 368 to 213 K (Figure S4b, Supporting Information). Thus, the UCPL should not be due to the thermal induced bandgap rearrangement,
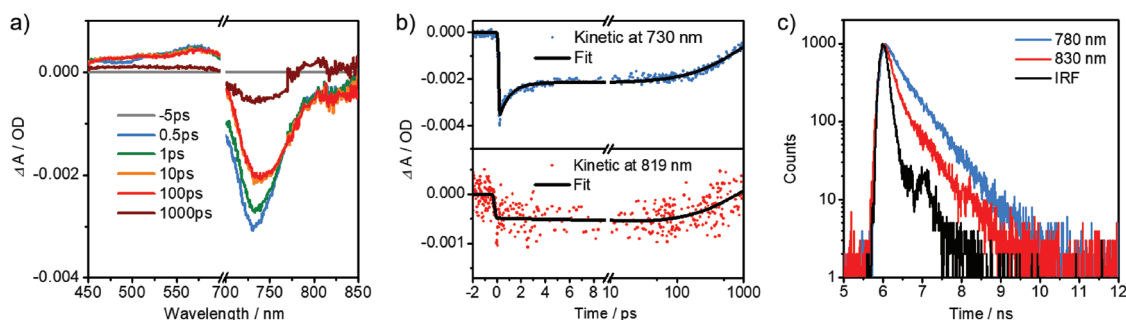
Figure 4. a) TA spectra of NIR-CDs in DMF at indicated delay times after excitation at λ_{pump} = 670 nm (1 KHz, 100 fs, around 1.5 μJ cm^{-2}). b) Bleach signal kinetics and corresponding fittings of NIR-CDs in DMF at 730 and 819 nm. c) PL decays of NIR-CDs in DMF collected at 780 and 830 nm with λ_{ex} = 808 nm. IRF is instrument response function.

but accounts for the thermally activated electron transitions in the excited state between the two optical emission bands in NIR-CDs around 760–800 and 820–880 nm, respectively. This assumption is confirmed by the temperature dependence of the UCPL integrated intensity at ≈760–800 nm compared to that of SPL at ≈820–880 nm, which is shown in Figure 3d. The UCPL/SPL intensity ratio increased with temperature following exponential dependence, $\exp(-\Delta E/k_BT)$. Similar UCPL was observed for NIR-CDs in other aprotic polar solvents such as N,N′-dimethylacetamide (DMA) and DMSO. When the NIR-CDs were dispersed in H_2O, no UCPL was detected. Thus, interactions of the electron-acceptor groups (C=O) with the single or few layer graphene-like cores of NIR-CDs should be the key factor to realize the UCPL in this system.

To further investigate the emission processes occurring in NIR-CDs, fs TA spectra and PL decay curves were collected. The TA spectra of NIR-CDs in DMF (**Figure 4**a,b) recorded upon the fs-pulse excitation at 670 nm show a broad intense ground-state bleaching (GSB) band peaked at ≈730 nm in the region of 700–800 nm (Band 1), followed by a weak GSB band in the region of 800–850 nm (Band 2). The TA kinetic traces probed at 730 and 819 nm are given in Figure 4b; both of them could be fitted by double-exponential functions. A rapid decay process at 730 nm occurs, accompanied with a rise component at 819 nm on the picosecond (ps) time scale (<13 ps), which indicates that the charge carrier transition takes place from the excited state of Band 1 to Band 2. It can be inferred that both the Band 1 and Band 2 should originate from the same CDs. The relatively long-lived components of 754 ps at 730 nm and 748 ps at 819 nm can be assigned to the radiative transitions. Under the excitation of 808 nm, the PL lifetimes of NIR-CDs at room temperature are in the range of hundreds of ps and are of 561 and 417 ps, when registered at 780 and 830 nm, respectively (Figure 4c). The observed PL spectrum consisting of two distinguished bands (Figure 3b), together with different PL lifetime registered at 780 and 830 nm indicate that the emission corresponds to the two discrete excited singlet states (S_1). Considering different chemical structures of the inner planes of the single-to-few layer graphene-like cores and the edges of NIR-CDs, the two fluorescence bands around 760–800 and 820–880 nm may originate from the DMF-solvent-mediated intrinsic state of the inner plane of the core and the DMF-solvent-bonded edge state of NIR-CDs, respectively. Correspondingly, the lowest energy structure of NIR-CD should feature

ground state "S_0" and two excited states, "S_1-int" (DMF-solvent-mediated intrinsic state) and "S_1-edge" (DMF-solvent-bonded edge state), which are spatially separated from each other with energy gap of ≈90–100 meV, which is in the same order of magnitude as that estimated from the temperature dependence of PL intensity redistribution between two excited states, shown in Figure 3d. A possible mechanism for the UCPL of NIR-CDs is illustrated in **Figure 5**. After absorbing the energy of the 808 nm laser, electrons are excited to the S_1-edge state, and then following two pathways for their radiative deactivation could be considered: (i) relaxation from the S_1-edge state to the ground state via SPL, or (ii) thermally activated upconversion from S_1-edge state followed by radiative relaxation from S_1-int to the ground state via UCPL. According to the observed temperature dependence of the intensity redistribution in the PL spectra (Figure 3c,d), the radiative energy dissipation through the path (ii) occurs at room temperature determined by thermal equilibrium, and becomes more predominant with rising temperature to thermally facilitate high electron population on S_1-int. Consequently, the energy dissipation through path (i) accounts for a smaller proportion compared with the path (ii) at and above room temperature. By contrast, upon cooling, path (i) plays an increasing role in the exciton deactivation compared with path (ii), resulting in SPL at low temperatures. Thus, thermally activated electron transitions from the excited state of the DMF-solvent-bond edge state to that of the DMF-solvent-mediated intrinsic state of single-to-few layer graphene-like cores account for the UCPL of NIR-CDs, which
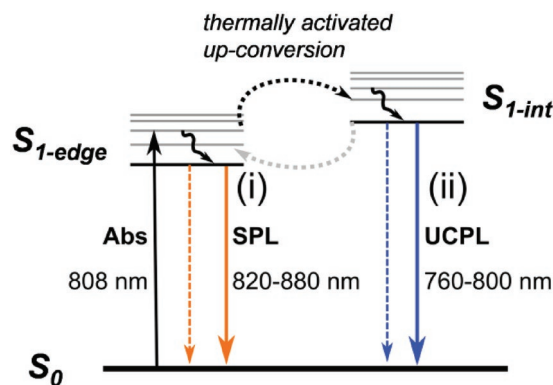
Figure 5. Schematic of the proposed mechanism of the UCPL in NIR-CDs.

is different from previously reported multiphoton absorption processes and hot band absorption processes occurring in CDs or organic dyes.[2a,7b,8f] Single-to-few layer NIR-CDs fabricated here may possess the increased degree of freedom of layer vibration resulting in increased probability of the electron transitions to higher energy levels in the excited state. Hence, the structural features of NIR-CDs not only contribute to the red-shifted optical spectra of NIR-CDs with their main absorption/emission in the NIR region, but are also responsible for the occurrence of NIR UCPL.

To the best of our knowledge, this is the first realization of thermally activated UCPL in CDs, which is different from the commonly observed multiphoton absorption mechanism;[8f] this property offers potential applications of NIR-CDs as imaging agents in the NIR upconversion luminescence imaging, where the NIR excitation can be realized by using easily available CW laser. As shown in Figure S5 (Supporting Information), a handwritten letter "L" composed of NIR-CDs dispersed in PVP (a C=O contained polymer) matrix can easily be imaged using a CMOS camera coupled with 770 nm short-pass optical filter under 808 nm CW laser excitation (irradiation power density: 9.6 mW cm^{-2}) at room temperature. By contrast, there is no fluorescence signal detected from the control letter "L" (right side of Figure S5, Supporting Information) composed of the bare PVP, under the same imaging conditions. This comparison confirms that the UCPL originates from the NIR-CDs embedded into PVP matrix. Subsequently, a temperature dependent NIR upconversion luminescence imaging has been carried out, and the continuously enhancing UCPL signal was captured from the letter "L" composed of the NIR-CD/PVP composite with the temperature increasing from 41 to 128 °C (**Figure 6**a), while upon cooling to room temperature, the signal has gradually decreased. Figure S6 (Supporting Information)

and Figure 6b show temperature dependent UCPL spectra (recorded through a 770 nm shortpass optical filter) of NIR-CDs embedded in a PVP film under 808 nm excitation, and the UCPL intensity at 740 nm as a function of the temperature. The UCPL intensity increased and then decreased when the temperature raised and went down, which well corresponds to the proposed thermally activated UCPL mechanism introduced above.

Using NIR-CDs as imaging agents, an exploration experiment showing the principal possibility of the in vivo NIR upconversion luminescence imaging has been conducted on a mouse model using a CMOS camera coupled with 770 nm shortpass optical filter. After subcutaneous injection of NIR-CDs in DMA (40 µL, 40 ppm) at room temperature, bright UCPL signal of NIR-CDs (Figure 6c) was captured on the back of the mouse under the excitation of 808 nm CW laser (irradiation power density: 9.6 mW cm^{-2}). Herein, considering the absence of any UCPL signal of NIR-CDs in water, a small amount of DMA (37.5 mg, dermal LD50: 7500 mg kg^{-1}) was used for injection into a mouse ($\approx$21 g) in the imaging experiment, because CDs exhibit well-defined UCPL in DMA (Figure S7, Supporting Information). Further experiments aimed on the exploration of the full potential of NIR-CDs as luminescence imaging agents including their long-term toxicity studies, and on conquering their UCPL quenching in water are in progress.

In summary, NIR absorbing/emissive CDs with thermally activated NIR UCPL have been synthesized through the microwave assisted thermal exfoliation of the red emissive CDs. The single-to-few-layer graphene-like structure of NIR-CDs has been identified by AFM and XRD; it offers a large contact area with electron-acceptor groups of the aprotic polar solvents (such as DMF), which results in the appearance of both the absorption and
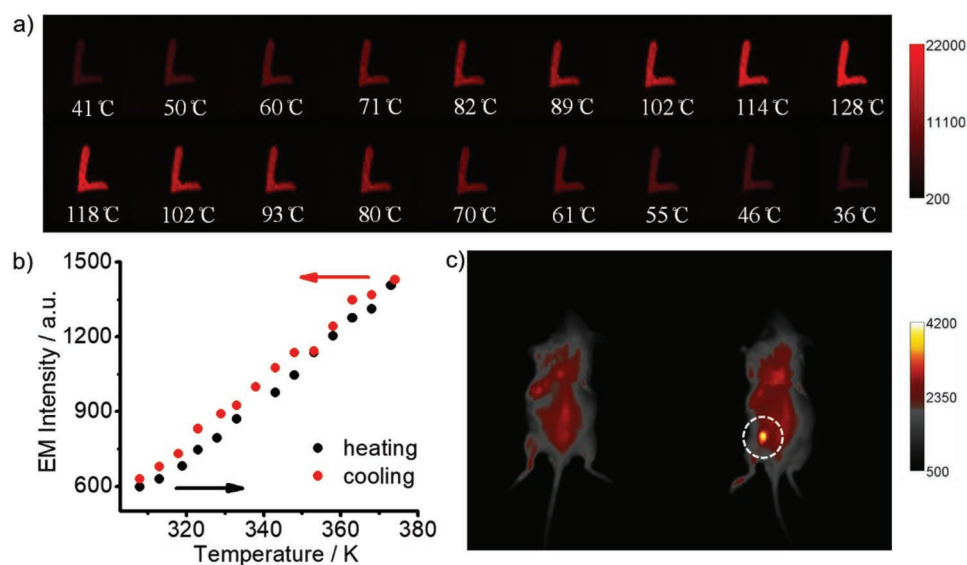
Figure 6. a) Temperature dependent NIR upconversion luminescence images of the letter "L" composed of NIR-CDs embedded in a PVP film during the heating (top frame) and cooling (bottom frame) processes. b) The UCPL intensity at 740 nm as a function of the temperature of NIR-CDs embedded in a PVP film measured through a 770 nm shortpass optical filter under 808 nm excitation during the heating and cooling processes. c) In vivo NIR upconversion luminescence images of a mouse before (left) and after (right) subcutaneous injection of NIR-CDs (excitation by 808 nm CW laser; emission is taken through the 770 nm shortpass optical filter).

emission in the NIR region. A mechanism involving thermally activated electron transitions in the excited state has been identified for the occurrence of UCPL of NIR-CDs. They can be conveniently excited by easily available continuous-wave NIR lasers, which is different from the previously reported multiphoton induced UCPL of CDs requiring the use of fs pulsed laser equipment. Exploring the NIR-CDs as an imaging agent, the temperature dependent NIR upconversion luminescence imaging has been demonstrated for NIR-CDs embedded into a PVP film, and their potential NIR upconversion luminescence imaging in vivo has been explored on a mouse model. The realization of thermally activated UCPL for CDs not only provides new insights into photophysical properties of CDs, but also introduces NIR-CDs as promising agent for NIR luminescence imaging.

Supporting Information

Supporting Information is available from the Wiley Online Library or from the author.

Acknowledgements

Conflict of Interest

The authors declare no conflict of interest.

Keywords

[1] a) R. Weissleder, *Nat. Biotechnol.* **2001**, *19*, 316; b) G. Hong, A. L. Antaris, H. Dai, *Nat. Biomed. Eng.* **2017**, *1*, 0010; c) V. J. Pansare, S. Hejazi, W. J. Faenza, R. K. Prud'homme, *Chem. Mater.* **2012**, *24*, 812.

[2] a) X. Zhu, Q. Su, W. Feng, F. Li, *Chem. Soc. Rev.* **2017**, *46*, 1025; b) G. Chen, H. Qiu, P. N. Prasad, X. Chen, *Chem. Rev.* **2014**, *114*, 5161.

[3] a) F. Auzel, *Chem. Rev.* **2004**, *104*, 139; b) H. Dong, S.-R. Du, X.-Y. Zheng, G.-M. Lyu, L.-D. Sun, L.-D. Li, P.-Z. Zhang, C. Zhang, C.-H. Yan, *Chem. Rev.* **2015**, *115*, 10725.

[4] a) M. Pawlicki, H. A. Collins, R. G. Denning, H. L. Anderson, *Angew. Chem., Int. Ed.* **2009**, *48*, 3244; b) R. K. Jain, C. Hu, T. K. Gustafson, S. S. Elliot, M. S. Chang, *J. Appl. Phys.* **1973**, *44*, 3157.

[5] a) L. M. Maestro, E. M. Rodríguez, F. S. Rodríguez, M. C. I.-d. la Cruz, A. Juarranz, R. Naccache, F. Vetrone, D. Jaque, J. A. Capobianco, J. G. Solé, *Nano Lett.* **2010**, *10*, 5109; b) D. J. Bharali, D. W. Lucey, H. Jayakumar, H. E. Pudavar, P. N. Prasad, *J. Am. Chem. Soc.* **2005**, *127*, 11364.

[6] a) L. Tu, X. Liu, F. Wu, H. Zhang, *Chem. Soc. Rev.* **2015**, *44*, 1331; b) G. Chen, C. Yang, P. N. Prasad, *Acc. Chem. Res.* **2013**, *46*, 1474.

[7] a) Y. P. Rakovich, J. F. Donegan, M. I. Vasilevskiy, A. L. Rogach, *Phys. Status Solidi A* **2009**, *206*, 2497; b) J. L. Clark, P. F. Miller, G. Rumbles, *J. Phys. Chem. A* **1998**, *102*, 4428; c) Y. P. Rakovich, S. A. Filonovich, M. J. M. Gomes, J. F. Donegan, D. V. Talapin, A. L. Rogach, A. Eychmüller, *Phys. Status Solidi B* **2002**, *229*, 449.

[8] a) S. N. Baker, G. A. Baker, *Angew. Chem., Int. Ed.* **2010**, *49*, 6726; b) K. Hola, Y. Zhang, Y. Wang, E. P. Giannelis, R. Zboril, A. L. Rogach, *Nano Today* **2014**, *9*, 590; c) L. Xiao, H. Sun, *Nanoscale Horiz.* **2018**, *3*, 565; d) Y. Yan, J. Gong, J. Chen, Z. Zeng, W. Huang, K. Pu, J. Liu, P. Chen, *Adv. Mater.* **2019**, *31*, 1808283; e) C. Ding, A. Zhu, Y. Tian, *Acc. Chem. Res.* **2014**, *47*, 20; f) G. E. LeCroy, S.-T. Yang, F. Yang, Y. Liu, K. A. S. Fernando, C. E. Bunker, Y. Hu, P. G. Luo, Y.-P. Sun, *Coord. Chem. Rev.* **2016**, *320–321*, 66; g) S. Qu, X. Wang, Q. Lu, X. Liu, L. Wang, *Angew. Chem., Int. Ed.* **2012**, *51*, 12215; h) D. Li, D. Han, S.-N. Qu, L. Liu, P.-T. Jing, D. Zhou, W.-Y. Ji, X.-Y. Wang, T.-F. Zhang, D.-Z. Shen, *Light: Sci. Appl.* **2016**, *5*, e16120.

[9] a) D. Li, P. Jing, L. Sun, Y. An, X. Shan, X. Lu, D. Zhou, D. Han, D. Shen, Y. Zhai, S. Qu, R. Zbořil, A. L. Rogach, *Adv. Mater.* **2018**, *30*, 1705913; b) X. Bao, Y. Yuan, J. Chen, B. Zhang, D. Li, D. Zhou, P. Jing, G. Xu, Y. Wang, K. Holá, D. Shen, C. Wu, L. Song, C. Liu, R. Zbořil, S. Qu, *Light: Sci. Appl.* **2018**, *7*, 91; c) H. Ding, J.-S. Wei, P. Zhang, Z.-Y. Zhou, Q.-Y. Gao, H.-M. Xiong, *Small* **2018**, *14*, 1800612; d) S. Lu, L. Sui, J. Liu, S. Zhu, A. Chen, M. Jin, B. Yang, *Adv. Mater.* **2017**, *29*, 1603443.

[10] a) L. Cao, X. Wang, M. J. Meziani, F. Lu, H. Wang, P. G. Luo, Y. Lin, B. A. Harruff, L. M. Veca, D. Murray, S.-Y. Xie, Y.-P. Sun, *J. Am. Chem. Soc.* **2007**, *129*, 11318; b) L. Pan, S. Sun, L. Zhang, K. Jiang, H. Lin, *Nanoscale* **2016**, *8*, 17350; c) S. Lu, G. Xiao, L. Sui, T. Feng, X. Yong, S. Zhu, B. Li, Z. Liu, B. Zou, M. Jin, J. S. Tse, H. Yan, B. Yang, *Angew. Chem., Int. Ed.* **2017**, *56*, 6187. d) Q. Liu, B. Guo, Z. Rao, B. Zhang, J. R. Gong, *Nano Lett.* **2013**, *13*, 2436.

[11] T.-F. Yeh, C.-Y. Teng, S.-J. Chen, H. Teng, *Adv. Mater.* **2014**, *26*, 3297.

[12] X. Li, X. Wang, L. Zhang, S. Lee, H. Dai, *Science* **2008**, *319*, 1229.

[13] a) F. Liu, M.-H. Jang, H. D. Ha, J.-H. Kim, Y.-H. Cho, T. S. Seo, *Adv. Mater.* **2013**, *25*, 3657; b) M. Zheng, L. Qiao, Y. Su, P. Gao, Z. Xie, *J. Mater. Chem. B* **2019**, *7*, 3840.